Science Advances

AAAS

advances.sciencemag.org/cgi/content/full/2/2/e1501145/DC1

Supplementary Materials for

Subtle balance of tropoelastin molecular shape and flexibility regulates dynamics and hierarchical assembly

Giselle C. Yeo, Anna Tarakanova, Clair Baldock, Steven G. Wise, Markus J. Buehler, Anthony S. Weiss

Published 5 February 2016, *Sci. Adv.* **2**, e1501145 (2016)
DOI: 10.1126/sciadv.1501145

This PDF file includes:

Other Supplementary Material for this manuscript includes the following:
(available at advances.sciencemag.org/cgi/content/full/2/2/e1501145/DC1)

Video S1 (.mpg format). The WT elastic network model displays a scissors-like motion between the hinge and foot regions, and a twisting motion in the N-terminal coil region.
Video S2 (.mpg format). The mutant WT+22 displays dynamics that significantly diverge from the WT.

SUPPLEMENTARY MATERIAL

Materials and methods

Mass spectrometry
WT and WT+22 (5 mg/mL in 0.1 M phosphate buffered saline, pH 7.4) were digested overnight at 25˚C with 0.05 mg/mL Lys-C (Calbiochem) and analyzed with matrix-assisted laser desorption ionization time-of-flight mass spectrometry using a QSTAR XL mass spectrometer (Applied Biosystems). Peaks were assigned by comparison with expected monoisotopic peptide masses from a theoretical Lys-C digest using PeptideMass (http://au.expasy.org/tools/peptide-mass.html).

Far-UV circular dichroism
CD spectra of 0.15 mg/mL WT and WT+22 tropoelastin in 10 mM phosphate and 150 mM NaF were recorded on a Jasco J-815 spectrometer equipped with a Peltier-controlled sample chamber. Samples were scanned with a bandwidth of 1.0 nm at 20 nm/min. Each spectrum was averaged from five scans, buffer-corrected, and smoothed using 3 point adjacent averaging. Secondary structure composition was estimated from the CD spectrum using the SELCON, CONTINLL and CDSSTR methods (*48*) with a reference set of 37 soluble proteins.

Replica exchange molecular dynamics (REMD)
REMD is a protein structure prediction method to improve conformational space sampling by combining molecular dynamics with the Monte Carlo method. The inputs used for Replica Exchange are the amino acid sequence and initial protein structure. We used a starting structure of an extended helical single-chain conformation of the amino acid sequence encoded by exons 21-23, with and without domain 22 inserted, based on a homology comparison method with the SCATCH Protein Predictor (*49*) that found discrete helical patterns in the systems. Starting configuration structures are assigned to different temperature replicas in a range. High temperature replicas ensure a wide conformational sampling while the ensemble of low temperature replicas is considered for structural prediction. Exchanges are made between neighboring replicas based on the Metropolis criterion, to allow for thermal stimulation of lower temperature replicas that may otherwise be trapped in a local free energy minimum state (*16, 39*). The exchange probability p between two replicas i and j, with temperatures T_i and T_j, and energies E_i and E_j, respectively, is (*16*):

$$p = \begin{cases} 1 & for\ \Delta \leq 0 \\ \exp(-\Delta) & for\ \Delta > 0 \end{cases} \quad (1)$$

where

$$\Delta = \left(\frac{1}{kT_i} - \frac{1}{kT_j}\right)(E_j - E_i) \quad (2)$$

After a sufficient number of exchanges, we consider an ensemble of structures at the lowest temperature for representative structure prediction.

Normal Mode Analysis
Molecular normal mode analysis is based on the assumption that a molecule will oscillate about an equilibrium configuration as a result of thermally induced fluctuations at the atomic scale. The molecule is coarsely modeled as a network of nodes interacting through simple harmonic

potentials, which can be visualized as a bead-spring system. Mathematically, the molecule is modeled as a system containing N interacting sites with coordinates q_i. The assumption in normal mode analysis maintains that the starting structure is an equilibrium orientation, such that ${q_i}^0$ are coordinates in the equilibrium configuration. The potential energy near equilibrium is approximated as:

$$V(q) = \frac{1}{2}\sum_{i,j}\left(\frac{\partial^2 V}{\partial q_i \partial q_j}\right)^0 (q_i - q_i^0)(q_j - q_j^0) \quad (3)$$

The terms $\left(\frac{\partial^2 V}{\partial q_i \partial q_j}\right)^0$ are components of the Hessian matrix. In the model of tropoelastin, the starting equilibrium configuration is derived from an average of small-angle x-ray scattering data. The interaction sites, or nodes, describe the topology of the native structure. The inter-nodal potential is defined by:

$$\phi_{\alpha\beta}(r) = \frac{1}{2}e^{\left(-\frac{r_{\alpha\beta}^2}{r_0^2}\right)}\left(r_{\alpha\beta} - r_{\alpha\beta}^0\right)^2 \quad (4)$$

The Hessian matrix is real and symmetric, such that upon diagonalization its eigenvectors form an orthonormal basis over the full space of molecular motion. Six of the eigenvalues are zero, indicative of rigid body rotations and translations of the molecule, having no effect on the internal potential energy of the system. Considering the molecule as a system of classically interacting particles, the equation of motion is:

$$\frac{d^2\Delta q}{dt^2} + H\Delta q = 0 \quad (5)$$

where M is the mass matrix, Δq are the coordinate components and H is the Hessian matrix. The equation of motion can be written as:

$$Hu_k = \omega_k^2 M u_k \quad (6)$$

assuming a solution of the form

$$u_k(t) = a_k \exp(-i\omega_k t) \quad (7)$$

This is a generalized eigenvalue problem, where the solution set u_k, with $1 \leq k \leq 3N$, and squared frequencies ω^2 represent the eigenvectors and eigenvalues, respectively. The eigenvectors of the mass-weighted Hessian matrix form an orthonormal basis set defining the normal modes of the molecule. The energy of a given mode can be written as

$$V(u_k) = \frac{1}{2}u_k^T H u_k = \frac{\omega_k^2}{2} \quad (8)$$

The energy of a mode is directly proportional to the eigenvalue, or the squared frequency of motion, $\lambda_k = \omega_k^2$. Thus, low-frequency modes are most accessible and least energetically expensive. Because the vibrational energy is equally distributed among the modes, the amplitude of oscillation for a given mode is inversely proportional to ω_k^2, making low-frequency modes most dominant within naturally occurring global molecular motion. A limitation to using SAXS-

derived structures for an equilibrium configuration of an elastic network model is an undefined mass distribution across the volume of the molecule. As a result, the model is simplified to a set of beads with equally partitioned mass.

Validation of the tropoelastin elastic network model

To validate the implementation of normal mode analysis with the elastic network model using SAXS-derived structures for WT and WT+22 tropoelastin, we compared the predictive efficacy of normal mode analysis for the 29-residue hinge region, with a SAXS-derived network model and a full-atomistic model with a complex potential function. The full-atomistic representative structure was identified with Replica Exchange Molecular Dynamics, implemented using the CHARMM c35b1r1 software package (*38, 50*) with the MMTSB toolset (*39*).The lowest free energy structure in the most statistically significant cluster was chosen as the representative equilibrium structure to conduct normal mode analysis. The CHARMM19 force field was used together with the eef1 implicit solvent model (*40*) to generate lowest-frequency eigenmodes and corresponding eigenvectors with the VIBRAN facility in the CHARMM implementation (*38*). An analogous elastic network model was created using volume-defining spatial coordinates from SAXS data (*20*) for the 29-residue hinge region. Nodal masses were uniform throughout the structure connected by distance-dependent springs, with stiffness similar to that used by Hinsen et al. (*19*):

$$k = C_1 e^{\left(-\frac{r^2}{r_0^2}\right)} \qquad (9)$$

where r_0 is the equilibrium inter-bead distance, r is the inter-bead distance, and a scaling factor C_1 set to 1. The anisotropic network model module in ProDy (*46*) was used.

The SAXS resolution of the domain 21/23 segment is higher than the full-length tropoelastin molecule, so we used a lower discretization (number of nodes) for the full-length molecule to define the bulk volume.

Because the vibrational energy is on average equally distributed among the modes (*51*), the amplitude of oscillation for each mode scales as the inverse of the frequency. We found a good correlation between modal displacement patterns of the full-atomistic and elastic network models independent of SAXS discretization. Additionally, we compared the elastic network model for a range of long-distance cutoff values defining the potential and found no significant difference to the full-atomistic complex potential model (Supplementary Fig S1G I, II).

Based on the normal mode analysis correlation between a SAXS-based network model and a full-atomistic resolution structure of the hinge region, we created a SAXS-based network model for the full tropoelastin molecule. Using a uniform space discretization derived from scattering data, we found a set of nodal coordinates to describe the volumetric shape of the molecule, as was done for the hinge region. Nodes represented by points of uniform mass were connected by springs with a distance-dependent spring constant, as in Equation 1. Normal mode analysis was conducted with the anisotropic network model function in ProDy simulation software (*46*).

Previous studies (*18, 19, 52, 53*) have shown that simplified potential models and coarser domain representations can capture the essential dynamics accessible to molecular systems. These observations result from the idea that the most biologically relevant, low frequency motions generally involve global subdomain displacements. Because small angle x-ray scattering captures the shape of such globular subdomains, it is not surprising that normal mode analysis with a SAXS-derived structure correlated highly with a full-atomistic normal mode analysis.

Coacervation assay
Light scattering of WT and WT+22 (10 mg/mL in 0.01 M PBS) was monitored by measuring absorbance at 300 nm over 600 s at 20-60˚C in a Shimadzu UV-1601 spectrophotometer. Between each temperature shift, the sample was cooled at 4˚C for 10 min. The constructs were assessed according to the time taken to reach maximum turbidity at each temperature and the temperature at which maximum sample turbidity was attained.

Particle size analysis
Dynamic light scattering of particle sizes in 10 mg/mL WT and WT+22 solutions were determined over a temperature range using a Malvern Zetasizer Nano (Malvern Instruments, UK). The tropoelastin solutions were equilibrated for 5 min at each temperature. At least 40 measurements were taken per sample and averaged to obtain the relative volume percentages of particle sizes in each solution.

WT+22 tropoelastin exhibits typical coacervation behavior
We wanted to determine whether the conformational shift in WT+22 affects its ability to undergo characteristic self-association. The entropy-driven aggregation of tropoelastin, known as coacervation, aligns the monomers for subsequent incorporation into elastic fibers and represents a commitment to elastogenesis (*54*). In salt and pH conditions approximating the extracellular environment, we found that WT+22 exhibits a temperature-dependent coacervation profile identical to WT, in which maximum solution turbidity is rapidly reached at physiological temperature (Supplementary Fig S2A). Within this critical temperature range of 35-40°C, WT+22 coacervated faster than WT, although the differences became minimal above 45°C (Supplementary Fig S2B). Analysis of particle sizes in the tropoelastin solutions confirmed the similar coacervation behavior of WT and WT+22 (Supplementary Fig S2C-F). Both species presented as ~10 nm monomers at 25 and 30°C, but sharply transited to ~1 μm multimers at 35°C and remained so at 40°C.

The temperature and rate of coacervation tightly correlate with protein hydropathy. Coacervation temperature reflects the energy required to disrupt clathrate water that shields hydrophobic domains from associating (*55*), while coacervation time relates to the cooperative association among hydrophobic regions (*56*). On this basis, addition of the hydrophobic domain 22 to tropoelastin did not alter protein hydration. However, we discovered that domain 22 contributes to a higher coacervation rate. Our observations can be explained by the altered WT+22 structure around the hinge and bridge regions, which may affect the positioning of central hydrophobic regions dominant in the coacervation process (*56*).

Cell attachment
Wells were coated with 1.25, 2.5, 5, 10, 20 or 30 μg/mL WT or WT+22 at 4˚C overnight then washed with PBS to remove unbound tropoelastin. Wells were blocked for 1 hr with 10 mg/mL denatured bovine serum albumin in PBS. Human dermal fibroblasts grown in Dulbecco's Modified Eagle Medium (DMEM) with 10% (v/v) fetal calf serum were pelleted and resuspended in serum-free DMEM. Wells were seeded at a density of 1.56×10^5 cells/cm^2. Standards with 10%, 20%, 50%, 80% and 100% of the seeding density were added to uncoated and unblocked wells. Cells were allowed to attach at 37˚C for 1 hr. Non-adherent cells were washed off while adhered cells were fixed with 3% (w/v) formaldehyde for 20 min and stained with 0.1% (w/v) crystal violet in 0.2 M MES, pH 5.0 for 1 hr. Excess stain was washed off with water, and the crystal violet was solubilized with 10% (w/v) acetic acid. The absorbances of the

standard wells at 570 nm were fitted to a linear regression and used to convert sample absorbances into percentage cell attachment.

Image analysis of elastic fibers

To compare fiber fluorescence, a threshold was set to exclude background and saturated pixel intensities. The average intensity of pixels within this threshold was measured for four fields of view per sample and averaged over triplicate samples. To compare fiber numbers, two perpendicular reference lines were drawn in each projection image. The number of fibers intersecting either reference line was counted for four fields of view per sample and averaged over triplicate samples. Fiber width was measured and averaged from ~150 randomly selected sections each of WT or WT+22 elastic fibers. Fiber area was measured by the percentage of fluorescent pixels over the total number pixels for four fields of view per sample, then averaged over triplicate samples. The area occupied by cell nuclei was used as a control of cell number and viability in all samples.

Supplementary figures

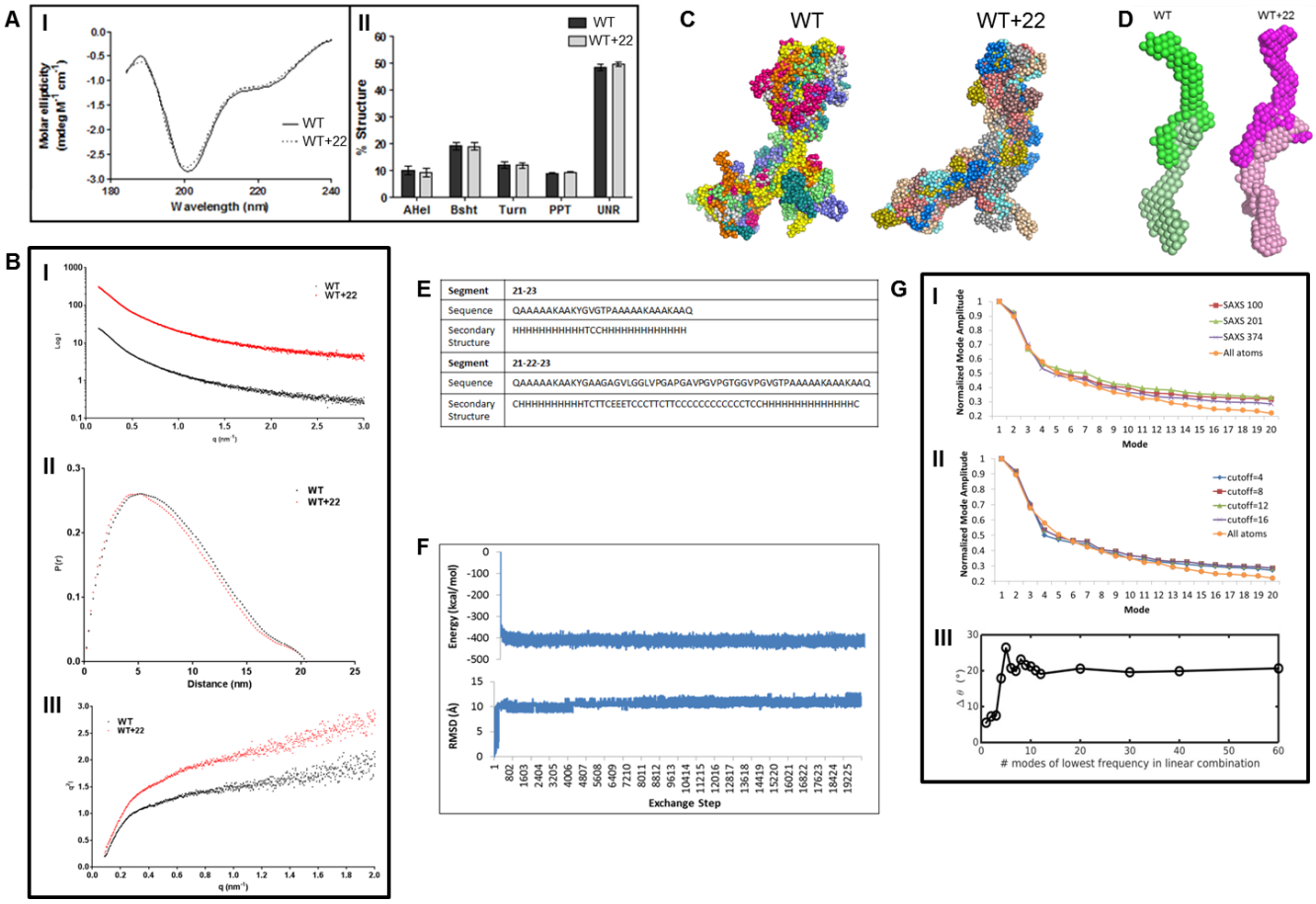

Fig. S1. Structure and dynamics of tropoelastin constructs. (**A**) Analysis of the overall secondary structure of tropoelastin. (I) Circular dichroism spectra of WT and WT+22. (II) Secondary structure composition of WT and WT+22 calculated from the CD spectra using SELCON, CONTINLL and CDSSTR algorithms. (**B**) SAXS measurements of WT and WT+22 showing (I) LogI vs q, (II) P(r) vs Distance, and (III) Kratky plots. The differences between the scattering profiles of WT and WT+22 are statistically significant (CorMap test, 1,024 points, C=152, p=0.0060) (*57*). (**C**) Alignment of WT and WT+22 shapes generated ab initio from multiple runs in GASBOR. These solutions were combined and filtered to obtain an average

model for each construct. (**D**) Model predicting possible head-to-tail tandem assembly of WT and WT+22 monomers. (**E**) Secondary structure predictions of hinge regions (domain 21/23 in WT and domain 21/22/23 in WT+22) based on homology modeling toolset SCRATCH. Sequences are in single letter amino acid code. Each residue is predicted to correspond to a secondary structure; one of alpha helix (H), turn (T), extended strand (E), or coil (C). (**F**) Potential energy and root mean square deviation (RMSD) from the original extended linear helical structure for the sequence encoded by domains 21/23, for 20,000 exchange steps, showing equilibration of the system. (**G**) (I) Normalized mode amplitudes for the first 20 modes for SAXS-derived structures of domain 21/23 in the hinge of WT tropoelastin (with 100, 201 and 374 beads representing the molecular volume) compared with the full-atomistic model. (II) Normalized mode amplitudes for the first twenty modes for the 374-bead structure of domain 21/23 in the hinge of WT tropoelastin with variations in cut-off distance compared with the full-atomistic model. (III) Change in theta for WT tropoelastin, defined as the angle between the legs of the molecule, representative of dynamics created by a varied number of lowest frequency modes in linear combination scaled by amplitude. Linear combination of six or higher number of modes results in nearly identical dynamics.

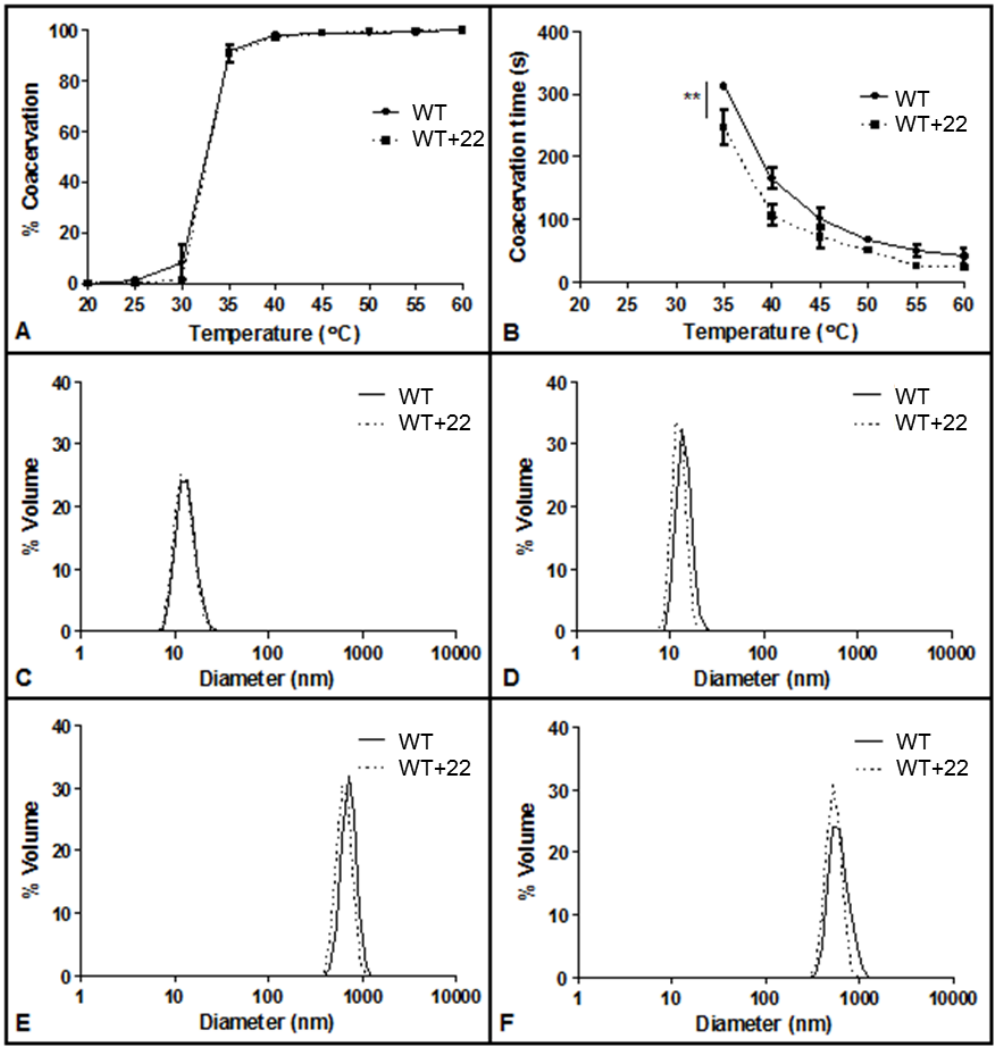

Fig. S2. Association by coacervation of WT and WT+22 tropoelastin solutions. (**A**) The extent of tropoelastin coacervation at each temperature. (**B**) The time taken to reach maximum coacervation at each temperature. (**C-F**) Analysis of the particle sizes within WT and WT+22 solutions at (C) 25, (D) 30, (E) 35, and (F) 40°C.

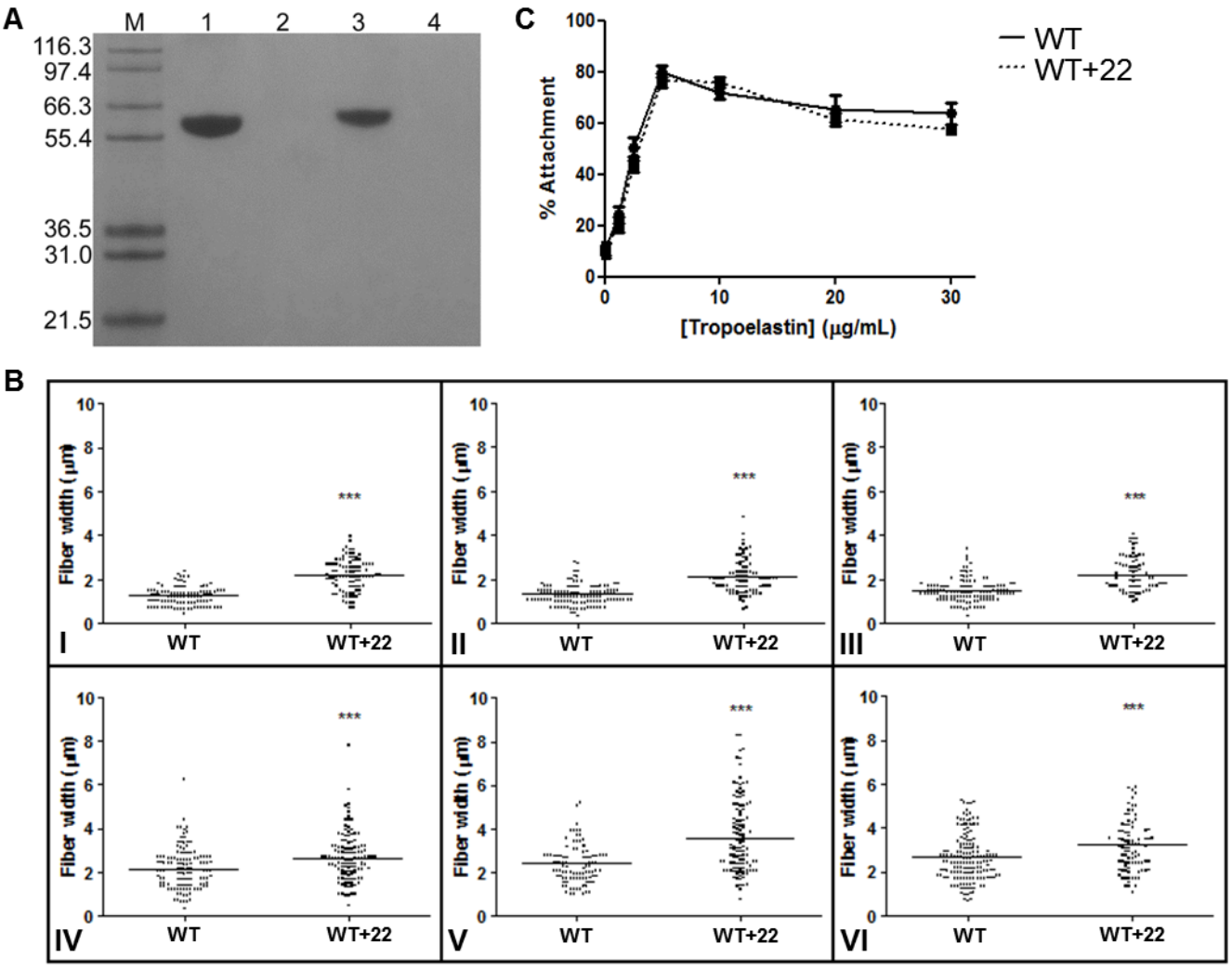

Fig. S3. Cross-linking, elastic fiber assembly, and cell attachment of tropoelastin constructs. (**A**) SDS-PAGE analysis of the extent of WT and WT+22 cross-linking. Lanes: M – Mark12 protein standards with sizes in kDa; 1 – WT; 2 – WT + 10 mM (6-fold molar excess) BS3; 3 – WT+22; 4 – WT+22 + 10 mM BS3 (6-fold molar excess). (**B**) Widths of WT and WT+22 elastic fibers formed by (I-III) 20 or (IV-VI) 200 µg/mL tropoelastin in ARPE-19 cells. Fibers were measured (I, IV) 4, (II, V) 7 and (III, VI) 10 days after tropoelastin addition. (**C**) Attachment of GM3348 human dermal fibroblasts to cell culture wells coated with various concentrations of WT and WT+22. The percentages of seeded cells which adhere to the tropoelastin coating are indicated.

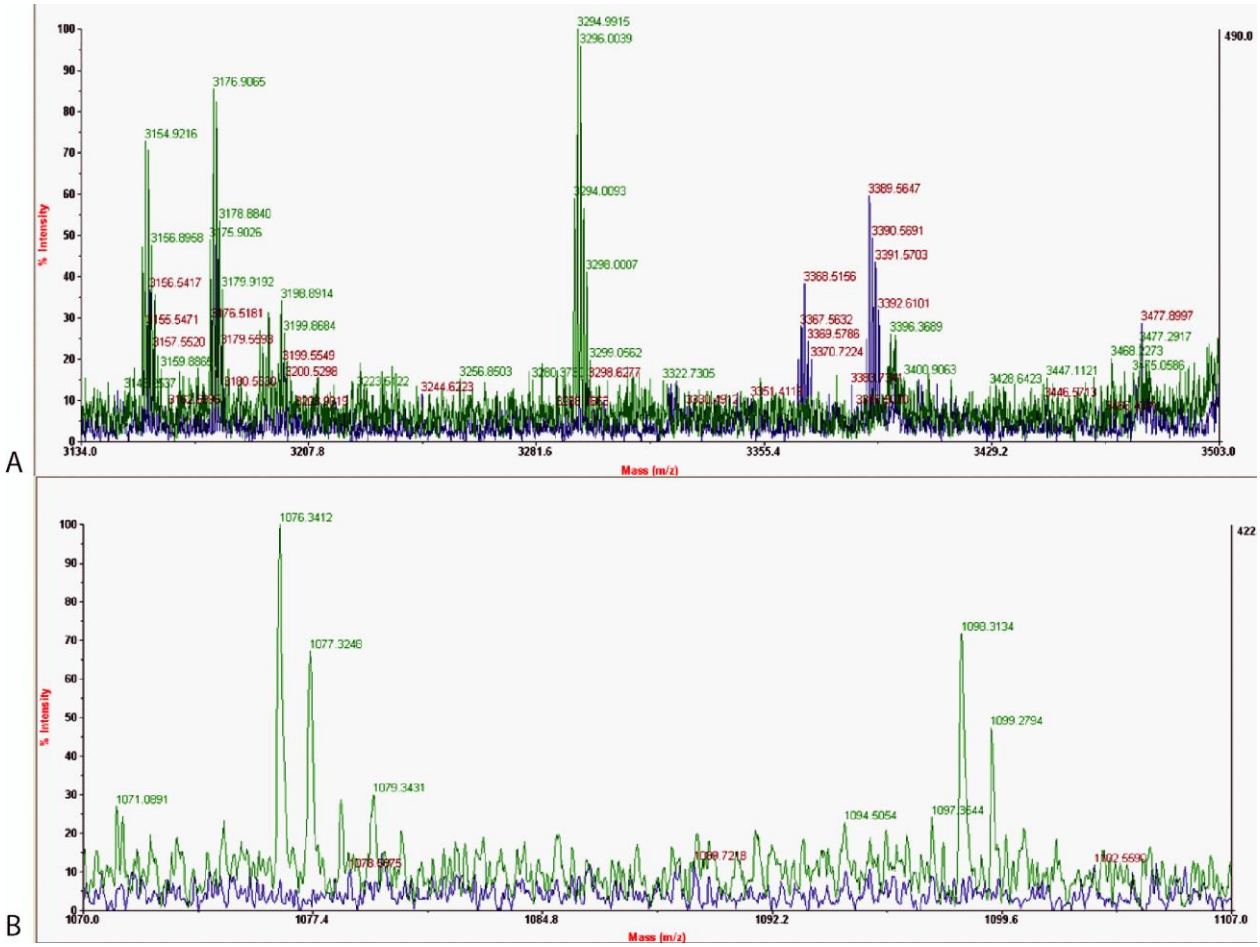

Fig. S4. Comparative mass spectrometry spectra of WT (green) and WT+22 (blue) tropoelastin. The mass profiles show the (**A**) disappearance of the WT-specific 1077 m/z peak and (**B**) appearance of the WT+22-specific 3367 m/z peak, which confirm the insertion of domain 22 within domains 21 and 23 in the mutant construct.

Supplementary Video 1. The WT elastic network model displays a scissors-like motion between the hinge and foot regions, and a twisting motion in the N-terminal coil region.

Supplementary Video 2. The mutant WT+22 displays dynamics that significantly diverge from the WT. Hinge and foot regions of the WT+22 molecule move in parallel, while the coil region bends along a perpendicular axis.